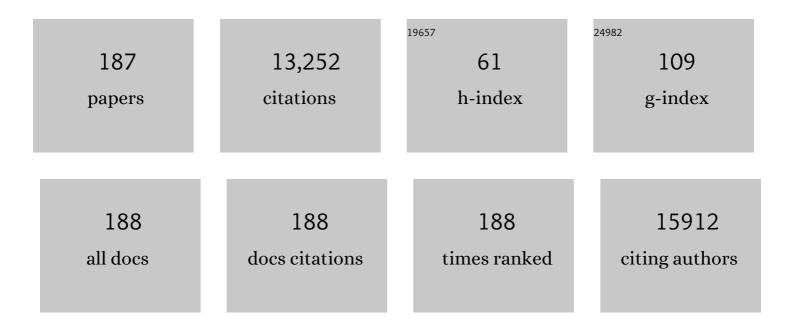
List of Publications by Year in descending order

Source: https://exaly.com/author-pdf/1639930/publications.pdf Version: 2024-02-01



Ιμνοινς Ημ

#	Article	IF	CITATIONS
1	Surface disorder engineering in ZnCdS for cocatalyst free visible light driven hydrogen production. Nano Research, 2022, 15, 996-1002.	10.4	50
2	Recent developments of infrared photodetectors with low-dimensional inorganic nanostructures. Nano Research, 2022, 15, 805-817.	10.4	13
3	In situ construction of heterostructured bimetallic sulfide/phosphide with rich interfaces for high-performance aqueous Zn-ion batteries. Science China Materials, 2022, 65, 356-363.	6.3	82
4	Tumor microenvironment responsive self-cascade catalysis for synergistic chemo/chemodynamic therapy by multifunctional biomimetic nanozymes. Journal of Materials Chemistry B, 2022, 10, 637-645.	5.8	18
5	Intracellular Mutual Amplification of Oxidative Stress and Inhibition Multidrug Resistance for Enhanced Sonodynamic/Chemodynamic/Chemo Therapy. Small, 2022, 18, e2107160.	10.0	57
6	Engineering DNA quadruplexes in DNA nanostructures for biosensor construction. Nano Research, 2022, 15, 3504-3513.	10.4	12
7	Ultrasmall AgBiSe <sub>2</sub> nanodots for CT/thermal imaging-guided photothermal tumor therapy in the NIR-II biowindow. Nanoscale, 2022, 14, 10750-10760.	5.6	2
8	Tumor Microenvironment Responsive Biodegradable Feâ€Doped MoO <i><sub>x</sub></i> Nanowires for Magnetic Resonance Imaging Guided Photothermalâ€Enhanced Chemodynamic Synergistic Antitumor Therapy. Advanced Healthcare Materials, 2021, 10, e2001665.	7.6	33
9	A high performance self-powered heterojunction photodetector based on NiO nanosheets on an n-Si (1 0 0) modified substrate. Materials Letters, 2021, 285, 128995.	2.6	8
10	Recent Progress of Methods to Enhance Photovoltaic Effect for Selfâ€Powered Heterojunction Photodetectors and Their Applications in Inorganic Lowâ€Dimensional Structures. Advanced Functional Materials, 2021, 31, 2011284.	14.9	66
11	Synthesis strategies and biomedical applications for doped inorganic semiconductor nanocrystals. Cell Reports Physical Science, 2021, 2, 100436.	5.6	14
12	An adjustable multi-color detector based on regulating TiO2 surface adsorption and multi-junction synergy. Nano Research, 2021, 14, 3423-3430.	10.4	9
13	A Near-Infrared Light Triggered Composite Nanoplatform for Synergetic Therapy and Multimodal Tumor Imaging. Frontiers in Chemistry, 2021, 9, 695511.	3.6	2
14	Programmable DNA Framework Sensors for In Situ Cell-Surface pH Analysis. Analytical Chemistry, 2021, 93, 12170-12174.	6.5	14
15	Dual-Modified Cu2S with MoS2 and Reduced Graphene Oxides as Efficient Photocatalysts for H2 Evolution Reaction. Catalysts, 2021, 11, 1278.	3.5	2
16	A simple method for preparing a TiO <sub>2</sub> -based back-gate controlled N-channel MSM–IGFET UV photodetector. Journal of Materials Chemistry C, 2020, 8, 1781-1787.	5.5	5
17	Solarâ€Inspired Water Purification Based on Emerging 2D Materials: Status and Challenges. Solar Rrl, 2020, 4, 1900400.	5.8	133
18	Controllable Hydrothermal Synthesis and Photocatalytic Performance of Bi2MoO6 Nano/Microstructures. Catalysts, 2020, 10, 1161.	3.5	15

#	Article	IF	CITATIONS
19	AgFeS <sub>2</sub> nanoparticles as a novel photothermal platform for effective artery stenosis therapy. Nanoscale, 2020, 12, 11288-11296.	5.6	15
20	Tumor environment responsive degradable CuS@mSiO2@MnO2/DOX for MRI guided synergistic chemo-photothermal therapy and chemodynamic therapy. Chemical Engineering Journal, 2020, 389, 124450.	12.7	124
21	Bioinspired, Microstructured Silk Fibroin Adhesives for Flexible Skin Sensors. ACS Applied Materials & Interfaces, 2020, 12, 5601-5609.	8.0	83
22	An efficiently enhanced UV-visible light photodetector with a Zn:NiO/p-Si isotype heterojunction. Journal of Materials Chemistry C, 2020, 8, 3498-3508.	5.5	17
23	In situ transmission electron microscope studies on one-dimensional nanomaterials: Manipulation, properties and applications. Progress in Materials Science, 2020, 113, 100674.	32.8	13
24	Probing the intermolecular interaction mechanisms between humic acid and different substrates with implications for its adsorption and removal in water treatment. Water Research, 2020, 176, 115766.	11.3	50
25	High-efficiency and safe sulfur-doped iron oxides for magnetic resonance imaging-guided photothermal/magnetic hyperthermia therapy. Dalton Transactions, 2020, 49, 5493-5502.	3.3	11
26	Oxygen vacancies-rich cobalt-doped NiMoO4 nanosheets for high energy density and stable aqueous Ni-Zn battery. Science China Materials, 2020, 63, 1205-1215.	6.3	71
27	Highly Ordered Mesoporous NiCo2O4 as a High Performance Anode Material for Li-Ion Batteries. Frontiers in Chemistry, 2019, 7, 521.	3.6	10
28	New Strategy for Specific Eradication of Implant-Related Infections Based on Special and Selective Degradability of Rhenium Trioxide Nanocubes. ACS Applied Materials & Interfaces, 2019, 11, 25691-25701.	8.0	21
29	Right Cu <sub>2â^'</sub> <i><sub>x</sub></i> S@MnS Core–Shell Nanoparticles as a Photo/H <sub>2</sub> O <sub>2</sub> â€Responsive Platform for Effective Cancer Theranostics. Advanced Science, 2019, 6, 1901461.	11.2	45
30	Reversible formation of networked porous Sb nanoparticles during cycling: Sb nanoparticles encapsulated in a nitrogen-doped carbon matrix with nanorod structures for high-performance Li-ion batteries. Journal of Materials Chemistry A, 2019, 7, 24292-24300.	10.3	23
31	Hierarchical assembly of manganese dioxide nanosheets on one-dimensional titanium nitride nanofibers for high-performance supercapacitors. Journal of Colloid and Interface Science, 2019, 552, 712-718.	9.4	25
32	CuCo <sub>2</sub> S <sub>4</sub> nanocrystals as a nanoplatform for photothermal therapy of arterial inflammation. Nanoscale, 2019, 11, 9733-9742.	5.6	37
33	Macrophages-Mediated Delivery of Small Gold Nanorods for Tumor Hypoxia Photoacoustic Imaging and Enhanced Photothermal Therapy. ACS Applied Materials & Interfaces, 2019, 11, 15251-15261.	8.0	71
34	Flower-like Fe <sub>7</sub> S <sub>8</sub> /Bi <sub>2</sub> S <sub>3</sub> superstructures with improved near-infrared absorption for efficient chemo-photothermal therapy. Dalton Transactions, 2019, 48, 3360-3368.	3.3	11
35	Hollow Co3O4@MnO2 Cubic Derived From ZIF-67@Mn-ZIF as Electrode Materials for Supercapacitors. Frontiers in Chemistry, 2019, 7, 831.	3.6	35
36	"All-in-One―Theranostic Agent with Seven Functions Based on Bi-Doped Metal Chalcogenide Nanoflowers. ACS Applied Materials & Interfaces, 2019, 11, 45467-45478.	8.0	24

#	Article	IF	CITATIONS
37	Janus Ag/Ag <sub>2</sub> S beads as efficient photothermal agents for the eradication of inflammation and artery stenosis. Nanoscale, 2019, 11, 20324-20332.	5.6	15
38	Biodegradable hollow manganese/cobalt oxide nanoparticles for tumor theranostics. Nanoscale, 2019, 11, 23021-23026.	5.6	35
39	A full-spectrum-absorption from nickel sulphide nanoparticles for efficient NIR-II window photothermal therapy. Nanoscale, 2019, 11, 20161-20170.	5.6	37
40	Fast Modulation of Surface Amphiphobicity/Amphiphilicity via Bidirectional Substitution between Perfluorinated Surfactants and Polyanions throughout Pre-Assembled Polyelectrolyte Multilayers. Langmuir, 2019, 35, 17122-17131.	3.5	6
41	Hierarchical multicomponent electrode with NiMoO4 nanosheets coated on Co3O4 nanowire arrays for enhanced electrochemical properties. Journal of Alloys and Compounds, 2019, 781, 1127-1131.	5.5	32
42	Improving the cycling stability of lithium–sulfur batteries by hollow dual-shell coating. RSC Advances, 2018, 8, 9161-9167.	3.6	3
43	A Dendritic Nickel Cobalt Sulfide Nanostructure for Alkaline Battery Electrodes. Advanced Functional Materials, 2018, 28, 1705937.	14.9	138
44	Stabilizing Lithium–Sulfur Batteries through Control of Sulfur Aggregation and Polysulfide Dissolution. Small, 2018, 14, e1703816.	10.0	28
45	Hydrophilic K <sub>2</sub> Mn <sub>4</sub> O <sub>8</sub> nanoflowers as a sensitive photothermal theragnosis synergistic platform for the ablation of cancer. New Journal of Chemistry, 2018, 42, 3714-3721.	2.8	9
46	Degradable rhenium trioxide nanocubes with high localized surface plasmon resonance absorbance like gold for photothermal theranostics. Biomaterials, 2018, 159, 68-81.	11.4	52
47	Synthesis of hollow NiCo2O4 nanospheres with large specific surface area for asymmetric supercapacitors. Journal of Colloid and Interface Science, 2018, 511, 456-462.	9.4	163
48	A facile method to fabricated UV–Vis photodetectors based on TiO2/Si heterojunction. Applied Surface Science, 2018, 449, 358-362.	6.1	19
49	Hierarchical hollow MnO2 nanofibers with enhanced supercapacitor performance. Journal of Colloid and Interface Science, 2018, 513, 448-454.	9.4	93
50	Facile synthesis of graphene nanoribbons from zeolite-templated ultra-small carbon nanotubes for lithium ion storage. Journal of Materials Chemistry A, 2018, 6, 21327-21334.	10.3	6
51	"Transformed―Fe <sub>3</sub> S <sub>4</sub> tetragonal nanosheets: a high-efficiency and body-clearable agent for magnetic resonance imaging guided photothermal and chemodynamic synergistic therapy. Nanoscale, 2018, 10, 17902-17911.	5.6	69
52	Cobalt nickel nitride coated by a thin carbon layer anchoring on nitrogen-doped carbon nanotube anodes for high-performance lithium-ion batteries. Journal of Materials Chemistry A, 2018, 6, 19853-19862.	10.3	38
53	An easy-to-fabricate clearable CuS-superstructure-based multifunctional theranostic platform for efficient imaging guided chemo-photothermal therapy. Nanoscale, 2018, 10, 11430-11440.	5.6	23
54	Porous cobalt sulfide hollow nanospheres with tunable optical property for magnetic resonance imaging-guided photothermal therapy. Nanoscale, 2018, 10, 14190-14200.	5.6	28

#	Article	IF	CITATIONS
55	Battery Electrodes: A Dendritic Nickel Cobalt Sulfide Nanostructure for Alkaline Battery Electrodes (Adv. Funct. Mater. 23/2018). Advanced Functional Materials, 2018, 28, 1870154.	14.9	7
56	Synthesis of hierarchical Co3O4@NiCo2O4 core-shell nanosheets as electrode materials for supercapacitor application. Journal of Alloys and Compounds, 2017, 700, 247-251.	5.5	57
57	CuCo <sub>2</sub> S <sub>4</sub> nanocrystals: a new platform for multimodal imaging guided photothermal therapy. Nanoscale, 2017, 9, 2626-2632.	5.6	47
58	Surface Coating Constraint Induced Anisotropic Swelling of Silicon in Si–Void@SiO <i><sub>x</sub></i> Nanowire Anode for Lithiumâ€ion Batteries. Small, 2017, 13, 1603754.	10.0	49
59	NixCo3â^'xS4@NiCo2O4 hybrid composites as supercapacitors electrode material. Materials Letters, 2017, 191, 101-104.	2.6	4
60	Treatment of steroid-induced osteonecrosis of the femoral head using porous Se@SiO2 nanocomposites to suppress reactive oxygen species. Scientific Reports, 2017, 7, 43914.	3.3	25
61	UV and visible light synergetic photodegradation using rutile TiO <sub>2</sub> nanorod arrays based on a p–n Junction. Dalton Transactions, 2017, 46, 4296-4302.	3.3	19
62	Enhanced adsorption capacity of ultralong hydrogen titanate nanobelts for antibiotics. Journal of Materials Chemistry A, 2017, 5, 4352-4358.	10.3	76
63	Design and Functionalization of the NIR-Responsive Photothermal Semiconductor Nanomaterials for Cancer Theranostics. Accounts of Chemical Research, 2017, 50, 2529-2538.	15.6	312
64	In situ transmission electron microscopy study of individual nanostructures during lithiation and delithiation processes. Journal of Materials Chemistry A, 2017, 5, 20072-20094.	10.3	27
65	A new strategy to effectively alleviate volume expansion and enhance the conductivity of hierarchical MnO@C nanocomposites for lithium ion batteries. Journal of Materials Chemistry A, 2017, 5, 21699-21708.	10.3	74
66	Enhanced UV-visible light photodetectors with a TiO <sub>2</sub> /Si heterojunction using band engineering. Journal of Materials Chemistry C, 2017, 5, 12848-12856.	5.5	61
67	Combined bortezomib-based chemotherapy and p53 gene therapy using hollow mesoporous silica nanospheres for p53 mutant non-small cell lung cancer treatment. Biomaterials Science, 2017, 5, 77-88.	5.4	59
68	Nanoparticles Encapsulated in Porous Carbon Matrix Coated on Carbon Fibers: An Ultrastable Cathode for Liâ€lon Batteries. Advanced Energy Materials, 2017, 7, 1601363.	19.5	48
69	A self-powered broadband photodetector based on an n-Si(111)/p-NiO heterojunction with high photosensitivity and enhanced external quantum efficiency. Journal of Materials Chemistry C, 2017, 5, 12520-12528.	5.5	71
70	An Interface Engineered Multicolor Photodetector Based on n‣i(111)/TiO <sub>2</sub> Nanorod Array Heterojunction. Advanced Functional Materials, 2016, 26, 1400-1410.	14.9	64
71	A novel and facile synthesis of porous SiO <sub>2</sub> -coated ultrasmall Se particles as a drug delivery nanoplatform for efficient synergistic treatment of cancer cells. Nanoscale, 2016, 8, 8536-8541.	5.6	50
72	Polypyrrole-encapsulated iron tungstate nanocomposites: a versatile platform for multimodal tumor imaging and photothermal therapy. Nanoscale, 2016, 8, 12917-12928.	5.6	34

#	Article	IF	CITATIONS
73	Hydrophilic bismuth sulfur nanoflower superstructures with an improved photothermal efficiency for ablation of cancer cells. Nano Research, 2016, 9, 1934-1947.	10.4	80
74	Electrochemical Energy Storage Application and Degradation Analysis of Carbon-Coated Hierarchical NiCo2S4 Core-Shell Nanowire Arrays Grown Directly on Graphene/Nickel Foam. Scientific Reports, 2016, 6, 20264.	3.3	56
75	Degradable Molybdenum Oxide Nanosheets with Rapid Clearance and Efficient Tumor Homing Capabilities as a Therapeutic Nanoplatform. Angewandte Chemie - International Edition, 2016, 55, 2122-2126.	13.8	254
76	Degradable Molybdenum Oxide Nanosheets with Rapid Clearance and Efficient Tumor Homing Capabilities as a Therapeutic Nanoplatform. Angewandte Chemie, 2016, 128, 2162-2166.	2.0	12
77	NaYF <sub>4</sub> :Yb/Er@PPy core–shell nanoplates: an imaging-guided multimodal platform for photothermal therapy of cancers. Nanoscale, 2016, 8, 1040-1048.	5.6	42
78	SnS nanosheets for efficient photothermal therapy. New Journal of Chemistry, 2016, 40, 4464-4467.	2.8	27
79	A Hybrid Electrode of Co3O4@PPy Core/Shell Nanosheet Arrays for High-Performance Supercapacitors. Nano-Micro Letters, 2016, 8, 143-150.	27.0	56
80	Synthesis of CuS nanoplate-containing PDMS film with excellent near-infrared shielding properties. RSC Advances, 2016, 6, 18881-18890.	3.6	26
81	Hierarchical core/shell structures of ZnO nanorod@CoMoO <sub>4</sub> nanoplates used as a high-performance electrode for supercapacitors. RSC Advances, 2016, 6, 3020-3024.	3.6	30
82	Hierarchical architectures of Co <sub>3</sub> O <sub>4</sub> ultrafine nanowires grown on Co <sub>3</sub> O <sub>4</sub> nanowires with fascinating electrochemical performance. New Journal of Chemistry, 2016, 40, 377-384.	2.8	7
83	Facile synthesis of 3D flower-like porous NiO architectures with an excellent capacitance performance. RSC Advances, 2015, 5, 47506-47510.	3.6	42
84	Hydrous RuO <sub>2</sub> nanoparticles as an efficient NIR-light induced photothermal agent for ablation of cancer cells in vitro and in vivo. Nanoscale, 2015, 7, 11962-11970.	5.6	44
85	Dendritic Heterojunction Nanowire Arrays for High-Performance Supercapacitors. Scientific Reports, 2015, 5, 7862.	3.3	82
86	Ethanol gas sensor based on a self-supporting hierarchical SnO <sub>2</sub> nanorods array. CrystEngComm, 2015, 17, 1800-1804.	2.6	12
87	Photothermal Theragnosis Synergistic Therapy Based on Bimetal Sulphide Nanocrystals Rather Than Nanocomposites. Advanced Materials, 2015, 27, 1339-1345.	21.0	149
88	One pot synthesis of nickel foam supported self-assembly of NiWO <sub>4</sub> and CoWO <sub>4</sub> nanostructures that act as high performance electrochemical capacitor electrodes. Journal of Materials Chemistry A, 2015, 3, 14272-14278.	10.3	167
89	Gold nanorods as a theranostic platform for in vitro and in vivo imaging and photothermal therapy of inflammatory macrophages. Nanoscale, 2015, 7, 13991-14001.	5.6	125
90	Three-dimensional-networked NiCo2S4 nanosheet array/carbon cloth anodes for high-performance lithium-ion batteries. NPG Asia Materials, 2015, 7, e195-e195.	7.9	158

#	Article	IF	CITATIONS
91	CuS@mSiO <sub>2</sub> -PEG core–shell nanoparticles as a NIR light responsive drug delivery nanoplatform for efficient chemo-photothermal therapy. Dalton Transactions, 2015, 44, 10343-10351.	3.3	80
92	Na <sub>0.3</sub> WO <sub>3</sub> nanorods: a multifunctional agent for in vivo dual-model imaging and photothermal therapy of cancer cells. Dalton Transactions, 2015, 44, 2771-2779.	3.3	27
93	An effective approach to reduce inflammation and stenosis in carotid artery: polypyrrole nanoparticle-based photothermal therapy. Nanoscale, 2015, 7, 7682-7691.	5.6	30
94	Heterostructures of CuS nanoparticle/ZnO nanorod arrays on carbon fibers with improved visible and solar light photocatalytic properties. Journal of Materials Chemistry A, 2015, 3, 7304-7313.	10.3	95
95	Design and synthesis of 3D hierarchical NiCo <sub>2</sub> S <sub>4</sub> @MnO <sub>2</sub> core–shell nanosheet arrays for high-performance pseudocapacitors. RSC Advances, 2015, 5, 44642-44647.	3.6	57
96	Highly ordered mesoporous NiCo <sub>2</sub> O <sub>4</sub> with superior pseudocapacitance performance for supercapacitors. Journal of Materials Chemistry A, 2015, 3, 11503-11510.	10.3	36
97	Mechanism analysis of the capacitance contributions and ultralong cycling-stability of the isomorphous MnO <sub>2</sub> @MnO <sub>2</sub> core/shell nanostructures for supercapacitors. Journal of Materials Chemistry A, 2015, 3, 6168-6176.	10.3	138
98	Molten Au/Ge Alloy Migration in Ge Nanowires. Nano Letters, 2015, 15, 2809-2816.	9.1	15
99	Growth of TiO <sub>2</sub> nanorod bundles on carbon fibers as flexible and weaveable photocatalyst/photoelectrode. RSC Advances, 2015, 5, 102868-102876.	3.6	27
100	Three-dimensional networked NiCo <sub>2</sub> O <sub>4</sub> /MnO <sub>2</sub> branched nanowire heterostructure arrays on nickel foam with enhanced supercapacitor performance. Journal of Materials Chemistry A, 2015, 3, 1717-1723.	10.3	94
101	High Detectivity Solarâ€Blind Highâ€Temperature Deepâ€Ultraviolet Photodetector Based on Multiâ€Layered ( <i>l</i> 00) Facetâ€Oriented <i>β</i> â€Ga <sub>2</sub> O <sub>3</sub> Nanobelts. Small, 2014, 10, 1848-185	6. <sup>10.0</sup>	185
102	A facile approach for the synthesis of Cu2â^'x Se nanowires and their field emission properties. Journal of Materials Science, 2014, 49, 532-537.	3.7	6
103	MnO <sub>2</sub> Nanoflower Arrays with High Rate Capability for Flexible Supercapacitors. ChemElectroChem, 2014, 1, 1003-1008.	3.4	48
104	Facile synthesis of hydrophilic polypyrrole nanoparticles for photothermal cancer therapy. Journal of Materials Science, 2014, 49, 3484-3490.	3.7	32
105	Hierarchical mesoporous NiCo2O4@MnO2 core–shell nanowire arrays on nickel foam for aqueous asymmetric supercapacitors. Journal of Materials Chemistry A, 2014, 2, 4795.	10.3	355
106	Cu7.2S4 nanocrystals: a novel photothermal agent with a 56.7% photothermal conversion efficiency for photothermal therapy of cancer cells. Nanoscale, 2014, 6, 3274.	5.6	239
107	Cu <sub>2â^'x</sub> Se@mSiO <sub>2</sub> –PEG core–shell nanoparticles: a low-toxic and efficient difunctional nanoplatform for chemo-photothermal therapy under near infrared light radiation with a safe power density. Nanoscale, 2014, 6, 4361-4370.	5.6	77
108	CoMoO <sub>4</sub> ·0.9H <sub>2</sub> O nanorods grown on reduced graphene oxide as advanced electrochemical pseudocapacitor materials. RSC Advances, 2014, 4, 34307.	3.6	46

#	Article	IF	CITATIONS
109	Self-assembled WO3â^'x hierarchical nanostructures for photothermal therapy with a 915 nm laser rather than the common 980 nm laser. Dalton Transactions, 2014, 43, 6244.	3.3	71
110	Design and synthesis of 3D interconnected mesoporous NiCo2O4@CoxNi1â^'x(OH)2 core–shell nanosheet arrays with large areal capacitance and high rate performance for supercapacitors. Journal of Materials Chemistry A, 2014, 2, 10090.	10.3	174
111	Sponge-like NiCo <sub>2</sub> O <sub>4</sub> /MnO <sub>2</sub> ultrathin nanoflakes for supercapacitor with high-rate performance and ultra-long cycle life. Journal of Materials Chemistry A, 2014, 2, 7738-7741.	10.3	69
112	Effect of temperature on the performance of ultrafine MnO <sub>2</sub> nanobelt supercapacitors. Journal of Materials Chemistry A, 2014, 2, 1443-1447.	10.3	108
113	Magnetic-field-assisted hydrothermal synthesis of 2 × 2 tunnels of MnO <sub>2</sub> nanostructures with enhanced supercapacitor performance. CrystEngComm, 2014, 16, 9987-9991.	2.6	27
114	MnMoO <sub>4</sub> ·4H <sub>2</sub> O nanoplates grown on a Ni foam substrate for excellent electrochemical properties. Journal of Materials Chemistry A, 2014, 2, 20723-20728.	10.3	111
115	Hydrothermal control growth of Zn2GeO4–diethylenetriamine 3D dumbbell-like nanobundles. CrystEngComm, 2014, 16, 3222.	2.6	17
116	Understanding the effect of polypyrrole and poly(3,4-ethylenedioxythiophene) on enhancing the supercapacitor performance of NiCo <sub>2</sub> O <sub>4</sub> electrodes. Journal of Materials Chemistry A, 2014, 2, 16731-16739.	10.3	70
117	Synthesis of Cu <sub>2</sub> ZnSnS <sub>4</sub> film by air-stable molecular-precursor ink for constructing thin film solar cells. RSC Advances, 2014, 4, 36046.	3.6	9
118	NiCo <sub>2</sub> O <sub>4</sub> Nanostructures as a Promising Alternative for NiO Photocathodes in pâ€Type Dyeâ€Sensitized Solar Cells with High Efficiency. Energy Technology, 2014, 2, 517-521.	3.8	29
119	Folic acid-conjugated hollow mesoporous silica/CuS nanocomposites as a difunctional nanoplatform for targeted chemo-photothermal therapy of cancer cells. Journal of Materials Chemistry B, 2014, 2, 5358.	5.8	88
120	A Novel Photothermal Nanocrystals of Cu7S4 Hollow Structure for Efficient Ablation of Cancer Cells. Nano-Micro Letters, 2014, 6, 169-177.	27.0	33
121	Hydrophilic Molybdenum Oxide Nanomaterials with Controlled Morphology and Strong Plasmonic Absorption for Photothermal Ablation of Cancer Cells. ACS Applied Materials & Interfaces, 2014, 6, 3915-3922.	8.0	166
122	Facile synthesis of biocompatible cysteine-coated CuS nanoparticles with high photothermal conversion efficiency for cancer therapy. Dalton Transactions, 2014, 43, 11709.	3.3	213
123	Exceptional pseudocapacitive properties of hierarchical NiO ultrafine nanowires grown on mesoporous NiO nanosheets. Journal of Materials Chemistry A, 2014, 2, 12799-12804.	10.3	52
124	Facile synthesis of porous MnCo <sub>2</sub> O <sub>4.5</sub> hierarchical architectures for high-rate supercapacitors. CrystEngComm, 2014, 16, 2335-2339.	2.6	131
125	Cover Picture: MnO2 Nanoflower Arrays with High Rate Capability for Flexible Supercapacitors		

#	Article	IF	CITATIONS
127	One-pot morphology-controlled synthesis of various shaped mesoporous silica nanoparticles. Journal of Materials Science, 2013, 48, 5718-5726.	3.7	49
128	Ni(OH) <sub>2</sub> /CoO/reduced graphene oxide composites with excellent electrochemical properties. Journal of Materials Chemistry A, 2013, 1, 478-481.	10.3	68
129	Melting of Metallic Electrodes and Their Flowing Through a Carbon Nanotube Channel within a Device. Advanced Materials, 2013, 25, 2693-2699.	21.0	23
130	Carbon-coated mesoporous NiO nanoparticles as an electrode material for high performance electrochemical capacitors. New Journal of Chemistry, 2013, 37, 4031.	2.8	44
131	Surface decoration of Bi2WO6 superstructures with Bi2O3 nanoparticles: an efficient method to improve visible-light-driven photocatalytic activity. CrystEngComm, 2013, 15, 9011.	2.6	75
132	Ultrathin PEGylated W <sub>18</sub> O <sub>49</sub> Nanowires as a New 980 nm‣aserâ€Driven Photothermal Agent for Efficient Ablation of Cancer Cells In Vivo. Advanced Materials, 2013, 25, 2095-2100.	21.0	370
133	Sub-10 nm Fe <sub>3</sub> O <sub>4</sub> @Cu <sub>2–<i>x</i></sub> S Core–Shell Nanoparticles for Dual-Modal Imaging and Photothermal Therapy. Journal of the American Chemical Society, 2013, 135, 8571-8577.	13.7	581
134	ZnO nanorods on reduced graphene sheets with excellent field emission, gas sensor and photocatalytic properties. Journal of Materials Chemistry A, 2013, 1, 8445.	10.3	193
135	Chain-like NiCo2O4 nanowires with different exposed reactive planes for high-performance supercapacitors. Journal of Materials Chemistry A, 2013, 1, 8560.	10.3	250
136	Self-assembling hybrid NiO/Co3O4 ultrathin and mesoporous nanosheets into flower-like architectures for pseudocapacitance. Journal of Materials Chemistry A, 2013, 1, 9107.	10.3	101
137	Arbitrary Multicolor Photodetection by Hetero-integrated Semiconductor Nanostructures. Scientific Reports, 2013, 3, 2368.	3.3	41
138	Nanocomposites: A Low-Toxic Multifunctional Nanoplatform Based on Cu9S5@mSiO2Core-Shell Nanocomposites: Combining Photothermal- and Chemotherapies with Infrared Thermal Imaging for Cancer Treatment (Adv. Funct. Mater. 35/2013). Advanced Functional Materials, 2013, 23, 4280-4280.	14.9	8
139	A Lowâ€Toxic Multifunctional Nanoplatform Based on Cu <sub>9</sub> S <sub>5</sub> @mSiO <sub>2</sub> Coreâ€5hell Nanocomposites: Combining Photothermal―and Chemotherapies with Infrared Thermal Imaging for Cancer Treatment. Advanced Functional Materials. 2013. 23. 4281-4292.	14.9	207
140	Construction of 980 nm laser-driven dye-sensitized photovoltaic cell with excellent performance for powering nanobiodevices implanted under the skin. Journal of Materials Chemistry, 2012, 22, 18156.	6.7	26
141	Heterostructures of vertical, aligned and dense SnO2 nanorods on graphene sheets: in situ TEM measured mechanical, electrical and field emission properties. Journal of Materials Chemistry, 2012, 22, 19196.	6.7	29
142	MnO2 ultralong nanowires with better electrical conductivity and enhanced supercapacitor performances. Journal of Materials Chemistry, 2012, 22, 14864.	6.7	101
143	Hydrophilic Cu2ZnSnS4 nanocrystals for printing flexible, low-cost and environmentally friendly solar cells. CrystEngComm, 2012, 14, 3847.	2.6	125
144	In situ preparation of CuInS2 films on a flexible copper foil and their application in thin film solar cells. CrystEngComm, 2012, 14, 1825.	2.6	32

#	Article	IF	CITATIONS
145	Phase-controlled synthesis and gas-sensing properties of zinc stannate (ZnSnO3 and Zn2SnO4) faceted solid and hollow microcrystals. CrystEngComm, 2012, 14, 2172.	2.6	89
146	A simple transformation from silica core–shell–shell to yolk–shell nanostructures: a useful platform for effective cell imaging and drug delivery. Journal of Materials Chemistry, 2012, 22, 17011.	6.7	37
147	In situ structural evolution from GeO nanospheres to GeO/(Ge, GeO2) core-shell nanospheres and to Ge hollow nanospheres. CrystEngComm, 2011, 13, 4611.	2.6	8
148	Morphology-selective synthesis and wettability properties of well-aligned Cu2-xSe nanostructures on a copper substrate. Journal of Materials Chemistry, 2011, 21, 3053.	6.7	32
149	Hydrothermal synthesis, growth mechanism, and properties of three-dimensional micro/nanoscaled hierarchical architecture films of hemimorphite zinc silicate. CrystEngComm, 2011, 13, 2273.	2.6	16
150	Silver nanotubes — Biopolymer-assisted hydrothermal synthesis. Canadian Journal of Chemistry, 2011, 89, 1245-1248.	1.1	0
151	One-pot synthesis of large-scaled Janus Ag–Ag2S nanoparticles and their photocatalytic properties. CrystEngComm, 2011, 13, 7189.	2.6	62
152	Highly aligned SnO2 nanorods on graphene sheets for gas sensors. Journal of Materials Chemistry, 2011, 21, 17360.	6.7	199
153	Lightly doped single crystalline porous Si nanowires with improved optical and electrical properties. Journal of Materials Chemistry, 2011, 21, 801-805.	6.7	47
154	SnO2 nanoribbons: excellent field-emitters. CrystEngComm, 2011, 13, 2289.	2.6	23
155	Uniform ZnSe microspheres self-assembled from ZnSe polyhedron shaped nanocrystals. CrystEngComm, 2011, 13, 1518-1524.	2.6	9
156	Recent Research on One-Dimensional Silicon-Based Semiconductor Nanomaterials: Synthesis, Structures, Properties and Applications. Critical Reviews in Solid State and Materials Sciences, 2011, 36, 148-173.	12.3	24
157	A controllable hydrothermal synthesis of uniform three-dimensional hierarchical microstructured ZnO films. CrystEngComm, 2011, 13, 6107.	2.6	14
158	High-precision, large-domain three-dimensional manipulation of nano-materials for fabrication nanodevices. Nanoscale Research Letters, 2011, 6, 473.	5.7	5
159	Hydrophilic Cu <sub>9</sub> S <sub>5</sub> Nanocrystals: A Photothermal Agent with a 25.7% Heat Conversion Efficiency for Photothermal Ablation of Cancer Cells <i>in Vivo</i> . ACS Nano, 2011, 5, 9761-9771.	14.6	1,155
160	A Mobile Sn Nanowire Inside a <i>βâ€</i> Ga <sub>2</sub> O <sub>3</sub> Tube: A Practical Nanoscale Electrically/Thermally Driven Switch. Small, 2011, 7, 3377-3384.	10.0	10
161	Hydrophilic Flower‣ike CuS Superstructures as an Efficient 980 nm Laserâ€Driven Photothermal Agent for Ablation of Cancer Cells. Advanced Materials, 2011, 23, 3542-3547.	21.0	760
162	A General Approach for the Growth of Metal Oxide Nanorod Arrays on Graphene Sheets and Their Applications. Chemistry - A European Journal, 2011, 17, 13912-13917.	3.3	66

#	Article	IF	CITATIONS
163	PEG-mediated solvothermal synthesis of NaYF4:Yb/Er superstructures with efficient upconversion luminescence. Journal of Alloys and Compounds, 2010, 506, L17-L21.	5.5	26
164	Controllable hydrothermal synthesis, growth mechanism, and properties of ZnO three-dimensional structures. New Journal of Chemistry, 2010, 34, 732.	2.8	39
165	New nanowire heterostructures: SnO <sub>2</sub> nanowires epitaxial growth on Si bicrystalline nanowires. CrystEngComm, 2010, 12, 89-93.	2.6	13
166	Single-crystal MgS nanotubes: synthesis and properties. CrystEngComm, 2010, 12, 1286-1289.	2.6	7
167	Large-scale, uniform, single-crystalline Cd(OH)2 hexagonal platelets for Cd-based functional applications. CrystEngComm, 2010, 12, 1726.	2.6	15
168	Excellent Field Emitters: Onion-Shaped Tipped Carbon Nanotubes. Journal of Physical Chemistry C, 2010, 114, 8282-8286.	3.1	6
169	Uniform, thin and continuous graphitic carbon tubular coatings on CdS nanowires. Journal of Materials Chemistry, 2009, 19, 1093.	6.7	7
170	Rapid Fabrication of Nanocrystals through in situ Electron Beam Irradiation in a Transmission Electron Microscope. Journal of Physical Chemistry C, 2009, 113, 5201-5205.	3.1	12
171	Prospective important semiconducting nanotubes: synthesis, properties and applications. Journal of Materials Chemistry, 2009, 19, 7592.	6.7	26
172	Rectangular or square, tapered, and single-crystal PbTe nanotubes. Journal of Materials Chemistry, 2009, 19, 3063.	6.7	12
173	Novel semiconducting nanowire heterostructures: synthesis, properties and applications. Journal of Materials Chemistry, 2009, 19, 330-343.	6.7	59
174	ZnO–Si side-to-side biaxial nanowire heterostructures with improved luminescence. Journal of Materials Chemistry, 2009, 19, 7011.	6.7	12
175	Large scaled hexagonal prismatic sub-micro sized Mg crystals by a vapor–liquid–solid process. Chemical Communications, 2009, , 4503.	4.1	3
176	Unconventional Ribbon-Shaped β-Ga <sub>2</sub> O <sub>3</sub> Tubes with Mobile Sn Nanowire Fillings. ACS Nano, 2008, 2, 107-112.	14.6	34
177	Carbon Nanotubes as Nanoreactors for Fabrication of Single-Crystalline Mg3N2Nanowires. Nano Letters, 2006, 6, 1136-1140.	9.1	67
178	Twinning in ultrathin silicon nanowires. International Journal of Materials Research, 2006, 97, 513-516.	0.3	2
179	Nanofabrication on ZnO nanowires. Applied Physics Letters, 2006, 89, 243111.	3.3	23
180	Fabrication of Metal-Semiconductor Nanowire Heterojunctions. Angewandte Chemie - International Edition, 2005, 44, 2140-2144.	13.8	52

#	Article	IF	CITATIONS
181	Temperature-Dependent Growth of Germanium Oxide and Silicon Oxide Based Nanostructures, Aligned Silicon Oxide Nanowire Assemblies, and Silicon Oxide Microtubes. Small, 2005, 1, 429-438.	10.0	52
182	Liquid Gallium Columns Sheathed with Carbon:  Bulk Synthesis and Manipulation. Journal of Physical Chemistry B, 2005, 109, 11580-11584.	2.6	13
183	Sn-Catalyzed Thermal Evaporation Synthesis of Tetrapod-Branched ZnSe Nanorod Architectures. Small, 2004, 1, 95-99.	10.0	79
184	Sn-Filled Single-Crystalline Wurtzite-Type ZnS Nanotubes. Angewandte Chemie - International Edition, 2004, 43, 4606-4609.	13.8	78
185	Synthesis and Field-Emission Properties of Ga2O3â^ C Nanocables. Chemistry of Materials, 2004, 16, 5158-5161.	6.7	40
186	Gallium Nitride Nanotubes by the Conversion of Gallium Oxide Nanotubes. Angewandte Chemie - International Edition, 2003, 42, 3493-3497.	13.8	93
187	Epitaxial Heterostructures:Â Side-to-Side Siâ^'ZnS, Siâ^'ZnSe Biaxial Nanowires, and Sandwichlike ZnSâ^'Siâ^'ZnS Triaxial Nanowires. Journal of the American Chemical Society, 2003, 125, 11306-11313.	13.7	124